Comparative Medicine
Copyright 2013
by the American Association for Laboratory Animal Science

Vol 63, No 2
April 2013
Pages 174–182

Original Research

Parenchymal Signal Intensity in 3-T Body MRI of Dogs with Hematopoietic Neoplasia

Daniel A Feeney,[1,*] Leslie C Sharkey,[1,2] Susan M Steward,[3] Katherine L Bahr,[1] Michael S Henson,[1,2] Daisuke Ito,[1,2] Timothy D O'Brien,[4] Carl R Jessen,[1] Brian D Husbands,[1] Antonella Borgatti,[1,2] and Jaime F Modiano[1,2]

We performed a preliminary study involving 10 dogs to assess the applicability of body MRI for staging of canine diffuse hematopoietic neoplasia. T1-weighted (before and after intravenous gadolinium), T2-weighted, in-phase, out-of-phase, and short tau inversion recovery pulse sequences were used. By using digital region of interest (ROI) and visual comparison techniques, relative parenchymal organ (medial iliac lymph nodes, liver, spleen, kidney cortex, and kidney medulla) signal intensity was quantified as less than, equal to, or greater than that of skeletal muscle in 2 clinically normal young adult dogs and 10 dogs affected with either B-cell lymphoma (*n* = 7) or myelodysplastic syndrome (*n* = 3). Falciform fat and urinary bladder were evaluated to provide additional perspective regarding signal intensity from the pulse sequences. Dogs with nonfocal disease could be distinguished from normal dogs according to both the visual and ROI signal-intensity relationships. In normal dogs, liver signal intensity on the T2-weighted sequence was greater than that of skeletal muscle by using either the visual or ROI approach. However in affected dogs, T2-weighted liver signal intensity was less than that of skeletal muscle by using either the ROI approach (10 of 10 dogs) or the visual approach (9 of 10 dogs). These findings suggest that the comparison of relative signal intensity among organs may have merit as a research model for infiltrative parenchymal disease (ROI approach) or metabolic effects of disease; this comparison may have practical clinical applicability (visual comparison approach) as well.

Abbreviations: RSI, relative signal intensity; MDS, myelodysplastic syndrome.

Canine malignant lymphoma is a multicentric, hematopoietic cancer that is very similar to nonHodgkin lymphoma in humans.[42,59] Both conditions are proportionally increasing as causes of mortality in the respective species.[21,42] The age-adjusted incidence of nonHodgkin lymphoma in dogs is 5 times that of humans.[42] The likelihood of survival after lymphoma treatment in dogs using accepted treatment protocols is highly dependent on initial staging and subsequent restaging.[59] Regardless of the underlying disease process or its distribution, focal or multifocal lesions represent measurable entities that can be monitored sequentially either clinically or with imaging techniques. However, diffuse disease, which occurs with no structural disruption (as in some round-cell neoplasias)[6,9,13] is problematic because there are no easily definable parameters other than changes in organ volume and (perhaps) signal intensity from which to differentiate normal from abnormal. The presence or absence of disease in the face of a metabolic reaction to a disease or its treatment can create staging and diagnostic dilemmas.[4,9,11,17,19,20,24,30,39,47,52]

Defining infiltrative disease with X-ray based technologies can be difficult because of the similarities in tissue density (g/mL^3) between normal and infiltrated tissues and the lack of focal lesions that may undergo differential contrast enhancement.[16] Ultrasound imaging techniques are based on the combined effects of reflections from the insonated tissues and attenuation by them combined with comparisons with the 'brightness' of other regional organs. This process provides insight into diffuse parenchymal organ infiltrates.[4,7,13,45,49,56,60,61,63] MRI has the combined advantages of imaging variances in tissue hydrogen mobility, detecting paramagnetic substances (gadolinium-based contrast agents, iron-based contrast agents, and extravascular blood products), melanin, and proteinaceous substances in tissues.[2,12,22,28,33,34,36,37,40,41,44,64]

Initial reports on whole-body MRI staging techniques in people indicate the potential to provide prognostically relevant information in a cost-effective, minimally invasive manner.[3,23,25,31,32,35,38,53,58] Whereas much of the attention on MRI techniques is focused on the detection and characterization of focal or multifocal disease, we found only limited information on diffuse or infiltrative parenchymal disease.[6,10,31,50] There has been notable interest in the applicability and accuracy of whole-body MRI, particularly related to the staging of multicentric and metastatic neoplastic disease in people,[3,23,25,31,32,35,48,53,58] with limited investigations in companion animals.[27] With infiltrative parenchymal organ malignancies, standard MRI detection may rely primarily on organ size or signal intensity instead of 'measurable' nodules or masses and may ultimately require diffusion characterization (for example, apparent diffusion coefficient) or ^{1}H spectroscopy.[15,26,48]

The underlying requirement for the interpretation of diffuse tissue or organ disease is an understanding of the normal appearance

Received: 02 Jul 2012. Revision requested: 16 Aug 2012. Accepted: 15 Nov 2012.
[1]Department of Veterinary Clinical Sciences, [2]The Masonic Cancer Center, [3]Veterinary Medical Center, and [4]Department of Veterinary Population Medicine, University of Minnesota, St Paul, Minnesota.
[*]Corresponding author. Email: feene001@umn.edu

and variation.[43] This knowledge is particularly noteworthy in MRI because of the differing signal intensities among parenchymal organs, body fluids, muscle types, and some specific infiltrates when imaged by using the broad array of available pulse sequences.[8,14,29,51,54,55] However, only limited information is available on normal relative organ and muscle MRI signal intensity, and even that information is limited to selected pulse sequences in people[1,5,46] or in small companion animals.[18,51] A region-of-interest–based, quantitative study of abdominal organ signal intensity in cats is available, but only with regard to T1- and T2-weighted sequences.[44] We believe this lack of relative organ signal intensity comparison is a hindrance to MRI investigation of infiltrative processes (for example, parenchymal lymphoma, early metastatic disease), the evaluation of pharmacologic effects (for example, chemotherapy), and the metabolic abnormalities created by the inciting disease (for example, excess liver fat or iron, extramedullary hematopoiesis) in dogs either as patients or as animal models for human disease. This information is particularly relevant to whole-body cancer screening or cancer staging endeavors with MRI.[23,31,32]

The purpose of this pilot study was to determine whether prospective data on a limited number of canine patients provided sufficient justification to further explore body MRI as an investigative approach for diffuse hematopoietic neoplasia for dogs as animal models of human disease or as clinical patients. The primary focus of this work was to provide initial insight regarding whether infiltrative canine hematopoietic neoplasia or its related metabolic consequences could be differentiated from features of clinically normal dogs by using a limited spectrum of 3-T MRI pulse sequences on the neck, thorax, abdomen, and pelvis that could be completed in less than 2 h.

Materials and Methods

Animals. Ten canine patients that presented to the University of Minnesota Veterinary Medical Center Oncology Service for staging and treatment of hematopoietic neoplasia underwent whole-body MR imaging. To be included, dogs had to have either cytologic or hematologic evidence of hematopoietic neoplasia. Dogs were excluded from consideration for the study they presented any unjustifiable risks associated with general anesthesia for the imaging procedure. All protocols were approved by the IACUC, and owner consent was obtained prior to the procedure. As a baseline, 2 clinically normal young dogs in the elective small animal surgery spay–neuter program underwent the same imaging protocol. Members of the anesthesiology service of the University of Minnesota Veterinary Medical Center induced and monitored general anesthesia in all dogs. In general, dogs were premedicated with butorphanol tartrate (0.2 to 0.6 mg/kg IM; Butorphic, Lloyd Laboratories, Shenandoah, IA) and dexmedetomidine hydrochloride (3.0 to 5.5 µg/kg IM; Dexdomitor, Orion Corporation, Espoo, Finland) and received propofol (2.6 to 6.6 mg/kg IV; PropoFlo, Abbott Laboratories, Chicago, IL) for anesthesia induction. Dogs were intubated and maintained under anesthesia during the MR scan by using inhalant isoflurane (IsoFlo, Abbott Laboratories).

Imaging. For imaging, the body was divided into cranial (excluding the head) and caudal halves, and the dogs were imaged by using 3.0-T equipment (3T HDX, General Electric Medical Systems, Milwaukee, WI) under general anesthesia without respiratory or cardiac gating. At least 2 of the 3 standard (dorsal, sagittal, transverse) imaging planes were obtained for each pulse sequence to permit orthogonal comparison. The pulse sequences used included T1-weighted fast spin-echo (repetition time, 825 ms; echo time, 20 ms; no. of excitations, 1), T2-weighted fast spin-echo [repetition time, 3200 ms; echo time, 120 ms; no. of excitations, 1), in-phase (repetition time, 140 ms; echo time, 2.1 ms; flip angle, 80°; no. of excitations, 1), out-of-phase (repetition time, 140 ms; echo time, 3.15 ms; flip angle, 80°; no. of excitations, 1], and short tau inversion recovery (STIR; repetition time, 3800 ms; echo time, 34 ms; inversion time, 160 ms; no. of excitations, 1). Slice thickness was 8 to 10 mm, with an interslice interval of 3 to 5 mm. The field of view was adjusted to body region imaged and ranged from 30 to 45 cm. The postGd sequence was a simple intravenous injection of gadodiamide (0.1 mmole/kg IV as a single bolus; Omniscan, General Electric Healthcare) followed by a T1-weighted fast spin-echo protocol. No specific effort was made to image arterial, tissue, venous, or wash-out phases. All pre-Gd sequences for both halves of the body were completed before any Gd was given. After administration of a single bolus of Gd-based contrast medium, the cranial and caudal halves of the body were imaged again over a span of about 30 min by using the T1-weighted protocol. The field of view was adjusted to body region imaged and ranged from 30 to 45 cm.

Image interpretation. All image interpretation was done without knowledge of bone marrow, lymph node, or parenchymal organ status other than that the dogs had suspected hematopoietic malignancy or were clinically normal. For each pulse sequence in each dog, relative signal intensity for fat, urinary bladder, skeletal muscle (lumbar paraspinal muscles), medial iliac lymph nodes, liver, spleen, kidney cortex, and kidney medulla were assessed visually according to a scale of 1 (the least signal-intense structure in the imaging region, excluding bone and air) to 8 (the most signal intense structure). In addition, user-defined regions of interest (ROI) from the MR images on a picture archive and communication system (Carestream Health, Rochester, NY) were identified for comparison with the visually defined signal-intensity relationships; to avoid bias, this assignment was not made in tandem with visual assessments. Each ROI for skeletal muscle, iliac lymph nodes, liver, spleen, kidney cortex, and kidney medulla was measured 3 times on each dog to limit partial volume effects and the average used for further comparison. A ratio was created for each organ (iliac lymph nodes, liver, spleen, kidney cortex, and kidney medulla) by dividing the average ROI for that organ for each dog by the average ROI for skeletal muscle for that same dog and pulse sequence. For comparison, the signal intensities in ROI for fat and urinary bladder each were measured once in the region of the bladder neck of each dog and were expressed as a ratio to that of skeletal muscle. The images for the signal-intensity comparisons were chosen and interpreted by one author (DF) to minimize partial volume artifact as well as include the greatest number of regional organs (for example, kidney, spleen, liver) possible from among simultaneous display of sagittal, transverse, and dorsal planes for both 2 body regions for each pulse sequence.

Bone marrow and lymph node sampling and evaluation. Bone marrow was sampled from 2 sites (iliac crest and proximal humerus) in each dog, unless directed otherwise by unexplainable or asymmetric findings on the MRI images. Bone marrow sampling was performed immediately after MRI. According to standard techniques, bone marrow aspirates were collected from each

site by using Rosenthal bone marrow aspirate needles, and core biopsies were obtained by using Jamshidi core biopsy needles. Cytologic diagnosis of lymphoma in a lymph node was defined as the presence of more than 50% medium to large or cytologically atypical lymphocytes. Bone marrow involvement in patients with lymphoma was diagnosed as the presence of greater than 2% lymphoblasts with a concurrent cytologic or histologic diagnosis of lymphoma in the periphery. The diagnosis of myelodysplastic syndrome (MDS) was based on a modification of the most recent World Health Organization scheme for myeloid neoplasms[57] that excludes the use of cytogenetic abnormalities, because these features have not been characterized in dogs. Briefly, the presence of refractory peripheral cytopenia in combination with evidence of dysplasia in greater than 10% of precursors in one or more myeloid lineages (erythroid, myeloid, or megakaryocytic) and a blast count of less than 20% resulted in a diagnosis of MDS.[62]

Comparisons among imaging, clinical and microscopic findings. The disease classifications were compared with the MRI findings in an attempt to find trends that would justify acquiring patient data suitable for statistical analysis in a subsequent study. Definable focal abnormalities in the parenchymal organs were measured when applicable. The relative signal intensities of the evaluated organs were compared between the clinically normal and affected dogs to see whether the disease (or its metabolic effects) created variations in relative signal intensity among the organs. Because of limited funding, the study was intended only as a proof of principle regarding whether parenchymal organ and lymph node abnormalities could be distinguished from comparable images on 2 clinically normal dogs. No statistical analyses were performed.

Results

Animals and diseases studied. The affected 10 dogs in the study had an average age of 7.9 y (range, 4.5 to 11 y) and included 5 neutered males (Akita, American Staffordshire terrier, Scottish terrier, Shetland sheepdog, standard poodle) and 5 spayed females (mixed breed, Shih Tzu, and 3 golden retrievers). The hematopoietic abnormalities identified were high-grade B cell lymphoma (n = 7) and MDS (n = 3). None of the dogs had prior steroid or cytotoxic therapy, except for one dog with MDS, which had been on systemic corticosteroid therapy for 84 d prior to MRI and bone marrow sampling. The 2 clinically normal young adult male dogs were approximately 1.5 and 3 y of age and had no exposure to steroids or chemotherapeutic drugs.

Regarding pathologic classification and staging information, 4 of the dogs with high-grade B-cell lymphoma had clinical stage 3a lymphoma, 1 had clinical stage 4a disease; and the remaining 2 had clinical stage 5a. The dog with stage 4a lymphoma had confirmed splenic involvement. One of the dogs with stage 5a lymphoma had cutaneous involvement, and the other had limited bone marrow involvement. By definition, all of the MDS dogs had bone marrow involvement.

Interpretation of relative MR signal intensity. The ratio of organ (renal medulla, renal cortex, liver, spleen, skeletal muscle, iliac lymph node) ROI signal intensity compared with regional skeletal muscle ROI signal intensity from the 10 affected dogs (averaged across all 10 dogs) and the 2 normal dogs (average of the 2 dogs) are listed in Table 1. For perspective, the ratios of fat to skeletal muscle and urinary bladder to skeletal muscle are also listed. Figure 1 includes representative dorsal images from a clinically normal dogs that were obtained by using preGd T1-weighted, postGd T1-weighted, T2-weighted, in-phase, out-of-phase, and STIR sequences. In general, the majority of the pulse sequences provided no discriminatory insight between the 2 clinically normal and the dogs affected with either lymphoma or MDS. However, on the T2-weighted sequence, ROI and visual signal intensity of liver was greater than that of regional skeletal muscle in both of the clinically normal dogs. In comparison, visual T2-weighted signal intensity of liver was less than or equal to that of regional skeletal muscle in 9 of the 10 affected dogs; a dog with lymphoma was the exception that resembled the normal dogs on visual assessment. However ROI liver signal intensity was less than that of skeletal muscle in all 10 of the affected dogs. Figures 2 and 3 are representative examples of these findings.

Several findings did not provide discriminatory value but may provide additional reference perspective for other studies using other sequences. These findings were consistent across both the ROI and visual assessments in nearly every instance. In both normal dogs and in all but one of the affected dogs (a lymphoma-affected dog), iliac lymph node signal intensities were greater than that of skeletal muscle on the STIR sequence (Figure 4). The spleens of both normal dogs and all but one of the affected dogs (an MDS-affected dog) had signal intensities less than that of skeletal muscle on images from the in-phase sequence. The livers of all but 2 (both lymphoma-affected dogs) of the 12 dogs had signal intensities greater than that of skeletal muscle on images from the out-of-phase sequence. All of the renal medullas (normal and affected) and all but 1 (a dog with lymphoma) of 12 dogs' renal cortices were brighter than skeletal muscle on the T2-weighted and STIR sequences. The remaining sequences yielded highly variable relationships between parenchymal and skeletal muscle signal intensities.

Only 2 dogs had focal parenchymal lesions (a 1-cm irregular nodule in the liver of one dog, and a 4-cm nodule in the spleen of another dog). Neither of the focal parenchymal lesions was sampled because the finding did not affect the diagnosis, and these were clinical patients with limitations regarding sampling.

Discussion

The ROI assessment of liver on T2-weighted images allowed the dogs with B-cell lymphoma or MDS to be distinguished from the normal dogs in this limited study. Similarly, the visual assessment of liver on T2-weighted images allowed all but one of the dogs with B-cell lymphoma and all of the MDS-affected dogs to be distinguished from the normal dogs. These observations suggest that the MR signal-intensity comparison approach has sufficient merit to justify further investigation of normal relationships in signal intensity among tissues and their comparison with diffuse infiltrative parenchymal disease in dogs as patients and as animal models of human disease. In addition, the use of skeletal muscle as a ready source for signal intensity for comparison seemed to have practical value in identifying parenchymal organ signal intensity relationships that differ between affected and normal dogs. The underlying question not answered by this study is whether the signal intensity differences found are due to malignant cell infiltrates, extramedullary hematopoiesis, tumor-induced metabolic perturbations, or just tissue hyperplasia. Because these were clinical patients in a research protocol, extensive sampling beyond that germane to routine clinical staging was not permitted. However, these variations do draw attention to

Table 1. Ratio of signal intensity (SI) by MR pulse sequence at 3 T of region of interest to that of skeletal muscle in 2 clinically normal dogs (Normal) compared with 7 dogs with B-cell lymphoma and 3 dogs with myelodysplastic syndrome (Affected)

	T1-weighted		T1-weighted after IV Gd contrast		T2-weighted		In-phase		Out-of-phase		Short tau inversion recovery	
SI ratio	Normal	Affected	Normal	Affected	Normal	Affected	Normal	Affected	Normal	Affected	Normal	Affected
0.4–0.49						Liver (0.47)						
0.5–0.59	Bladder (0.54)	Liver (0.59)							Bladder (0.59)			
0.6–0.69	Liver (0.61)	Bladder (0.62)	Liver (0.62)	Liver (0.67)			Bladder (0.60)	Bladder (0.62)		Bladder (0.66)		
0.7–0.79							Spleen (0.73)	Spleen (0.73)	Spleen (0.75)	Spleen (0.73)		
								Medulla (0.74)				
0.8–0.89			Bladder (0.83)				Medulla (0.86)	Cortex (0.83)	Medulla (0.83)	Node (0.88)		
							Node (0.86)		Node (0.88)	Medulla (0.89)	Fat (0.85)	Liver (0.89)
0.9–0.99							Cortex (0.93)	Node (0.91)				
1.00	Muscle (1.00)	Muscle (1.00)	Muscle (1.00)	Muscle (1.00)	Muscle (1.00)	Muscle (1.00)	Muscle (1.00)	Muscle (1.00)	Muscle (1.00)	Muscle (1.00)	Muscle (1.00)	Muscle (1.00)
1.01–1.25	Medulla (1.05)	Cortex (1.01)		Bladder (1.24)				Liver (1.14)	Cortex (1.04)	Cortex (1.06)		Fat (1.22)
		Medulla (1.02)		Spleen (1.24)						Liver (1.13)		
		Spleen (1.03)										
1.26–1.50	Cortex (1.40)	Node (1.28)	Spleen (1.44)		Liver (1.36)				Liver (1.36)		Liver (1.26)	
	Spleen (1.47)											
1.51–1.75			Node (1.75)	Node (1.58)			Liver (1.57)			Fat (1.59)	Spleen (1.72)	
1.76–1.99	Node (1.79)			Cortex (1.75)		Spleen (1.85)		Fat (1.94)	Fat (1.79)			Spleen (1.78)
2.00–2.25							Fat (2.16)				Cortex (2.08)	
2.26–2.50			Cortex (2.50)	Medulla (2.28)							Node (2.40)	Cortex (2.27)
2.51–2.75				Fat (2.61)		Node (2.60)					Bladder (2.57)	Node (2.52)
2.76–2.99		Fat (2.80)	Medulla (2.98)			Cortex (2.86)					Medulla (2.94)	
3.00–3.99	Fat (3.72)		Fat (3.34)		Node (3.89)							Medulla (3.54)
4.00–4.99					Spleen (4.64)	Medulla (4.86)						Bladder (4.28)
5.00–5.99					Cortex (5.44)	Fat (5.46)						
6.00–6.99						Bladder (6.30)						
7.00–7.99					Bladder (7.62)							
8.00–8.99					Fat (8.23)							
9.00–9.99					Medulla (9.66)							

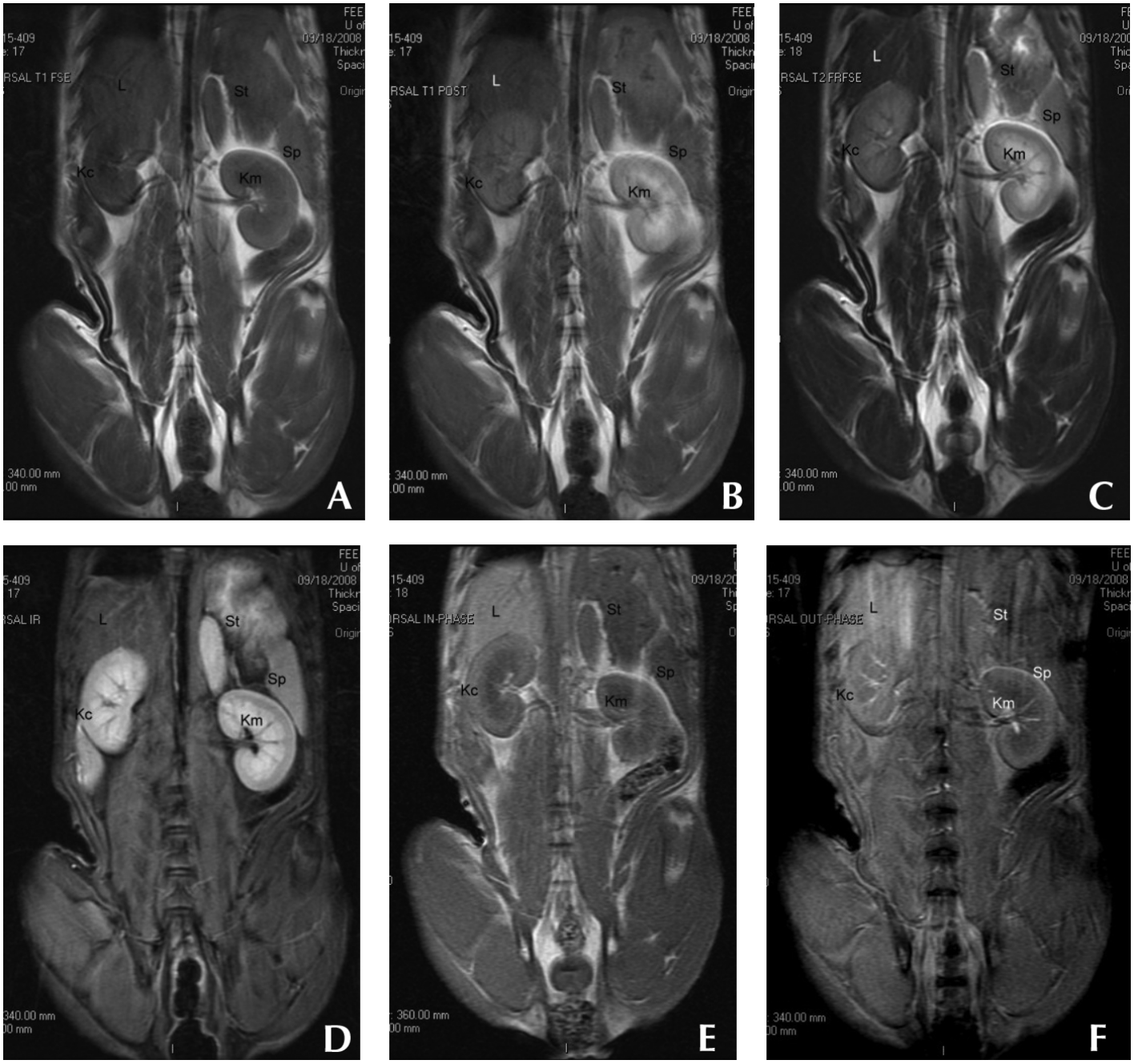

Figure 1. Dorsal-plane MR images from a clinically normal young adult dog that were obtained by using (A) preGd T1-weighted, (B) postGd T1-weighted, (C) T2-weighted, (D) STIR, (E) in-phase, and (F) out-of-phase pulse sequences. Variations in relative organ signal intensity can be seen among abdominal organs. Kc, kidney cortex; Km, kidney medulla; L, liver; Sp, spleen; St, stomach wall.

potential abnormalities that may merit further investigation in clinical patients.

The 2 clinically normal dogs were included for feasibility assessment of using MR signal intensity as part of the interpretive background for whole-body imaging of infiltrative disease (disease that does not alter the tissue or organ architecture) that could be performed in less than 2 h by using multiple sequences and without complex gating instrumentation or induced respiratory paralysis and mechanical ventilation. The goal was to have a protocol that was sufficiently practical to be used in either research or clinical applications. Although some artifacts were introduced due to respiratory and cardiac motion, these did not render the studies uninterpretable.

Visually apparent differences in relative tissue brightness were present not only across the pulse sequences in clinically normal dogs but also between the clinically normal and the abnormal dogs within pulse sequences in the current study. This observation could be exploited if, on verification of normal parenchymal signal-intensity variation and microscopic verification of the type of cellular infiltrates, this difference was found to be associated

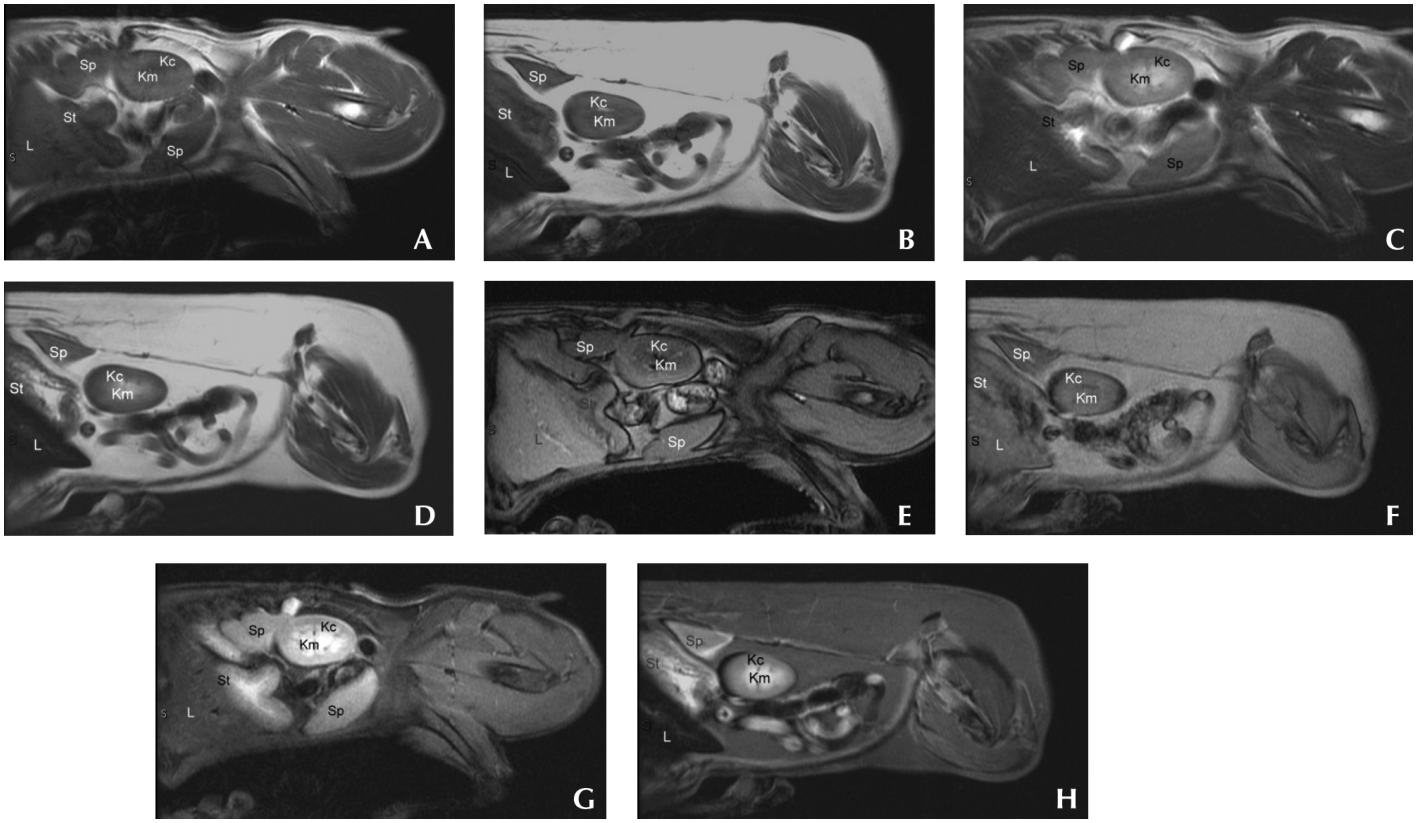

Figure 2. Left sagittal abdominal MR images from a clinically normal dog (A, C, E, G) and a dog with myelodysplasic syndrome (B, D, F, H) that were obtained by using (A, B) preGd T1-weighted, (C, D) T2-weighted, (E, F) out-of-Phase, and (G, H) STIR sequences. Differences in the relative signal intensity of the abdominal parenchymal organs are apparent. Kc, kidney cortex; Km, kidney medulla; L, liver; Sp, spleen; St, stomach (labeled to minimize confusion between liver and spleen). Note the comparatively lower signal relative signal intensity of the liver of the dog with MDS.

with either infiltrative malignancies or the abnormal metabolic states induced by malignant conditions. The finding of unexpected differences in relative tissue brightness may be a clue to underlying disease states, much like that seen with ultrasonography of parenchymal organs. That the liver signal intensity on in-phase and out-of-phase sequences was greater than that of skeletal muscle in both of the normal and most of the affected dogs limits the likelihood that simple iron deposition[2] is the explanation for this finding but requires additional investigation.

Our choice of pulse sequences focused on standard T1-weighted pre- and post-contrast and T2-weighted sequences because of their application in routine clinical MRI. In addition, the out-of-phase, in-phase, and STIR protocols were included to determine what effect variations in relative fat content had on the appearance of normal tissues, metabolic perturbations induced by the neoplastic process, or the effects of the known hematopoietic neoplasia. Gradient echo sequences were not chosen because the intent of the study was not specifically iron detection.[2] Diffusion-weighted sequences were not used because of the complexity of their application in nongated (respiratory or cardiac) animals.[48,58] For the abdominal parenchymal organs, we found little applicability of the in-phase, out-of-phase, and STIR protocols in distinguishing affected from normal dogs, except that the STIR protocol improved the visibility of lymph nodes. However, with further study of other infiltrative malignant processes including early, nonnodular metastatic disease, these sequences may yet provide insight.

We used the visual approach to evaluation of signal intensity because of its clinical practicality. The ROI analyses were used to provide quantification. It is our opinion that the only clinical applicability of the ROI approach is to clarify isolated instances, because applying this approach across several organs on multiple pulse sequences is too involved for routine clinical interpretation. The causes of variation between the visual and ROI approaches in several organs were at least partly attributable to the tissue being used for comparison. To limit bias, we did not perform the ROI and visual analyses in tandem, and this constraint adds credibility to the comparison between liver and skeletal muscle as being indicative of either malignant or metabolic abnormalities because the 2 analyses were nearly congruent. Our observations suggest that absolute numeric ROI assessments vary between patients; we therefore constructed Table 1 by using skeletal muscle as an internal standard for comparison. The ROI-based ratios almost always paralleled the visual assessments of relative signal intensity among the organs. In addition, machine-to-machine variation in absolute signal intensity likely outweighs the utility of anything other than assessment of relative signal intensity. However, signal intensity relationships should remain constant across MR equipment of similar field strength.

Several next steps are involved in evaluating the comparison of parenchymal MR signal intensity in dogs for research and clinical applications. First, a detailed study of normal parenchymal signal intensity relationships and the expected variation is necessary. Second, a prospective detailed sampling of all organs and tissues

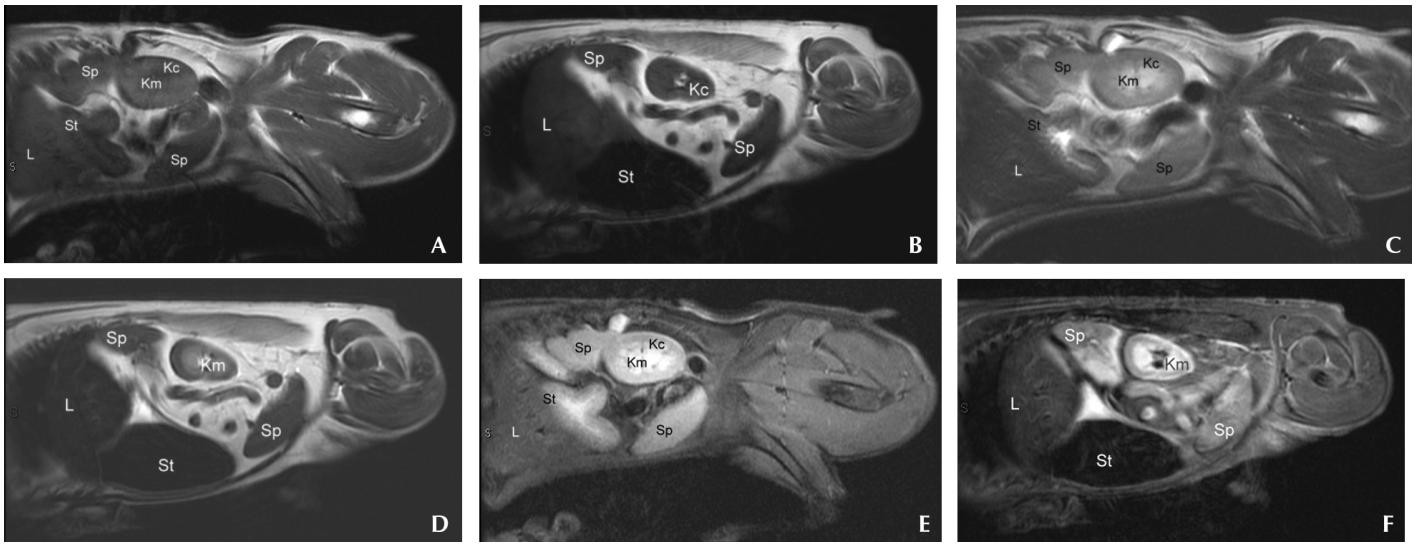

Figure 3. Left sagittal abdominal MR images from a clinically normal dog (A, C, E) and a dog with stage 5a high-grade B-cell lymphoma (B, D, F) that were obtained by using (A, B) preGd T1-weighted, (C, D) T2-weighted, and (E, F) STIR sequences. Differences in the relative signal intensity of the abdominal parenchymal organs are apparent. Kc, kidney cortex; Km, kidney medulla; L, liver; Sp, spleen; St, stomach (labeled to minimize confusion between liver and spleen). Note the comparatively lower relative T2-weighted signal intensity of the liver of the dog with lymphoma.

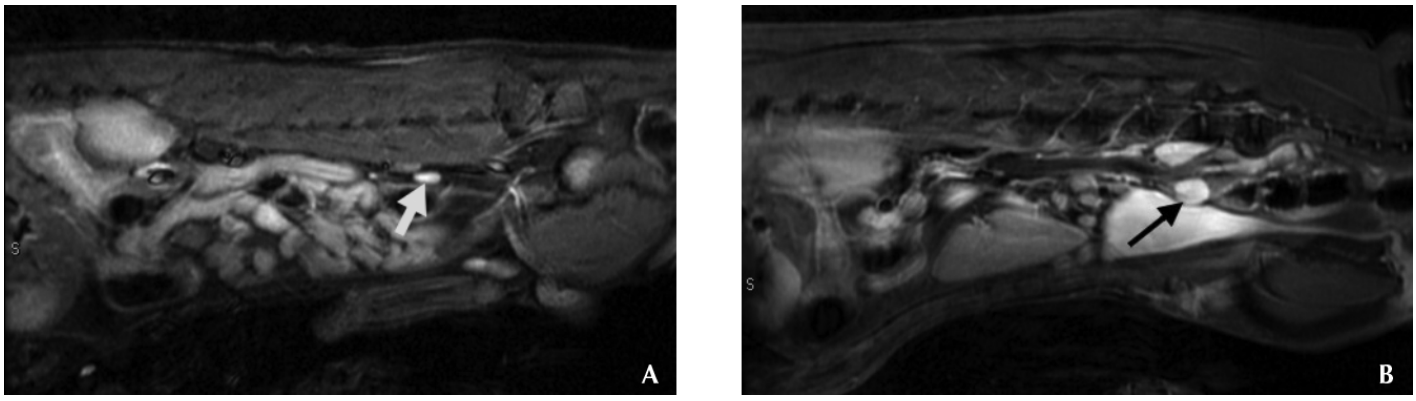

Figure 4. Sagittal MR images from (A) a clinically normal dog and (B) a dog with stage 3a high-grade B-cell lymphoma that were obtained by using the STIR sequence for evaluation of the medial iliac lymph nodes (arrows). Note the high signal intensity of the nodes in both dogs and the visibly larger nodes in the dog with lymphoma.

with signal intensities beyond those expected in normal dogs should be performed to determine whether the observed signal intensity variations are due to parenchymal neoplastic infiltration or the metabolic effects of the hematopoietic neoplastic process. Finally, the visual signal intensity approach must be compared across a series of interpreters to determine whether this approach has clinical applicability in parenchymal organ MRI interpretation in the same manner as relative organ echogenicity in diagnostic ultrasonography. Because of its pilot nature and limited numbers of normal and affected dogs, the current study was not intended as a test of reproducibility for the visual signal intensity approach across multiple interpreters, and was not intended to be blinded in regard to normal compared with abnormal dogs.

In conclusion, despite the small numbers of clinically normal and affected dogs that we evaluated, comparison of parenchymal signal intensity facilitated differentiation of dogs affected with selected hematopoietic malignancies from dogs that were clinically normal by either visual or ROI methods. In light of the data that we obtained, we suggest that this approach may yield germane information about infiltrative parenchymal disease if visible signal intensity stratification is addressed during research using animal models or during clinical interpretation of dogs with potentially infiltrative hematopoietic malignancies. In addition, using a combination of signal intensity criteria across organs may increase the reliability of diffuse disease evaluation. Additional advantages may be identifying those patients in whom more detailed parenchymal organ sampling may be justified and revealing a parenchymal abnormality at the edge of an imaged target region (for example, a liver abnormality seen during MRI of the spine), thereby perhaps influencing the next steps in the clinical work-up. This study has implications not only for the dog as an MR imaging model for diffuse hematopoietic neoplasia in people because of its other similarities to the condition in humans[42] but also for its potential applicability to clinical assessment of infiltrative malignancies in dogs as companion animals.

References

1. **Akisik FM, Sandrasegaran K, Aisen AM, Lin C, Lall C.** 2007. Abdominal MR imaging at 3.0 T. Radiographics **27:**1433–1444.
2. **Alustiza JM, Castiella A, De Juan MD, Emparanza JI, Artetxe J, Uranga M.** 2007. Iron overload in the liver diagnostic and quantification. Eur J Radiol **61:**499–506.
3. **Barth MM, Smith MP, Pedrosa I, Lenkinski RE, Rofsky NM.** 2007. Body MR imaging at 3.0 T: understanding the opportunities and challenges. Radiographics **27:**1445–1462.
4. **Biller DS, Kantrowitz B, Miyabayashi T.** 1992. Ultrasonography of diffuse liver disease. A review. J Vet Intern Med **6:**71–76.
5. **Bydder GM, Chung CB.** 2009. Magnetic resonance imaging of short T2 relaxation components in the musculoskeletal system. Skeletal Radiol **38:**201–205.
6. **Colagrande S, Centi N, Galdiero R, Ragozzino A.** 2007. Transient hepatic intensity differences: part 2, those not associated with focal lesions. Am J Roentgenol **188:**160–166.
7. **Crews LJ, Feeney D, Jessen CR, Rose ND.** 2009. Clinical, ultrasonographic, and laboratory findings associated with gall bladder disease and rupture in dogs: 45 cases (1997–2007). J Am Vet Med Assoc **234:**359–366.
8. **Cronin CG, Lohan DG, Browne AM, Roche C, Murphy M.** 2009. Magnetic resonance enterography in the evaluation of the small bowel. Semin Roentgenol **44:**237–243.
9. **Danrad R, Martin DR.** 2005. MR imaging of diffuse liver diseases. Magn Reson Imaging Clin N Am **13:**277–293.
10. **de Bazelaire CM, Duhamel GD, Rofsky NM, Alsop DC.** 2004. MR imaging relaxation times of abdominal and pelvic tissues measured in vivo at 3.0 T: preliminary results. Radiology **230:**652–659.
11. **Delorme S, Baur-Melnyk A.** 2009. Imaging in multiple myeloma. Eur J Radiol **70:**401–408.
12. **Do RK, Rusinek H, Taouli B.** 2009. Dynamic contrast-enhanced MR imaging of the liver: current status and future directions. Magn Reson Imaging Clin N Am **17:**339–349.
13. **Feeney DA, Anderson KL, Ziegler LE, Jessen CR, Daubs BM, Hardy RM.** 2008. Statistical relevance of ultrasonographic criteria in the assessment of diffuse liver disease in dogs and cats. Am J Vet Res **69:**212–221.
14. **Fenchel M, Kramer U, Nael K, Miller S.** 2007. Cardiac magnetic resonance imaging at 3.0 T. Top Magn Reson Imaging **18:**95–104.
15. **Fischbach F, Schirmer T, Thormann M, Freund T, Ricke J, Bruhn H.** 2008. Quantitative proton magnetic resonance spectroscopy of the normal liver and malignant hepatic lesions at 3.0 Tesla. Eur Radiol **18:**2549–2558.
16. **Flohr TG, Schaller S, Stierstofer K, Bruder H, Ohnesorge BM, Schoepf UJ.** 2005. Multi-detector row CT systems and image reconstruction techniques. Radiology **235:**756–773.
17. **Gagne JM, Armstrong PJ, Weiss DJ, Lund EM, Feeney DA, King VL.** 1999. Clinical features of inflammatory liver disease in cats: 41 cases (1983–1993). J Am Vet Med Assoc **214:**513–516.
18. **Gavin PR, Holmes S.** 2009. Magnetic resonance imaging of abdominal disease, p 273–293. In: Gavin PR, Bagle RS, editors. Practical small animal MRI. Ames (IA): Wiley–Blackwell.
19. **Gilad R, Milillo P, Som P.** 2007. Severe diffuse systemic amyloidosis with involvement of the pharynx, larynx, and trachea: CT and MR findings. Am J Neuroradiol **28:**1557–1558.
20. **Gorg C, Bert T.** 2005. Pictorial review: sonographic patterns of diffuse and focal fatty infiltration of the liver: Differential diagnosis to metastatic liver disease. Onkologie **28:**659–664.
21. **Jemal A, Tiwari RC, Murray T, Ghafoor A, Samuels A, Ward E, Feurer E, Thun MJ.** 2004. Cancer statistics, 2004. Cancer J Clin **54:**8–29.
22. **Jeudy J, White CS.** 2008. Cardiac magnetic resonance imaging: techniques and principles. Semin Roentgenol **43:**173–182.
23. **Johnston C, Brennan S, Ford S, Eustace S.** 2006. Whole-body MR imaging: applications in oncology. Eur J Surg Oncol **32:**239–246.
24. **Joseph AE, Savarymuttu SH, al-Sam S, Cook MG, Maxwell JD.** 1991. Comparison of liver histology with ultrasonography in assessing diffuse liver disease. Clin Radiol **43:**26–31.
25. **Kellenberger CJ, Epelman M, Miller SF, Babyn PS.** 2004. Fast STIR whole-body MR imaging in children. Radiographics **24:**1317–1330.
26. **Kingsley PB, Shah TC, Woldenberg R.** 2006. Identification of diffuse and focal brain lesions by clinical magnetic resonance spectroscopy. NMR Biomed **19:**435–462.
27. **Kraft S, Randall E, Wilhelm M, Lana S.** 2007. Development of a whole-body magnetic resonance imaging protocol for normal dogs and canine cancer patients. Vet Radiol Ultrasound **48:**212–220.
28. **Kuhn JP, Hegenscheid K, Siegmund W, Froehlich P, Hosten N, Puls R.** 2009. Normal dynamic MRI enhancement patterns of the upper abdominal organs: gadoxetic acid compared with gadobutrol. Am J Roentgenol **193:**1318–1323.
29. **Kuo R, Panchal M, Tanenbaum L, Crues JV.** 2007. 3.0-Tesla imaging of the musculoskeletal system. J Magn Reson Imaging **25:**245–261.
30. **Kwee TC, Kwee RM, Verdonck LF, Bierings MB, Nievelstein RA.** 2008. Magnetic resonance imaging for the detection of bone marrow involvement in malignant lymphoma. Br J Haematol 1**41:**60–68.
31. **Ladd SC, Ladd ME.** 2007. Perspectives for preventive screening with total-body MRI. Eur Radiol **17:**2889–2897.
32. **Lauenstein TC, Semelka RC.** 2006. Emerging techniques: whole-body screening and staging with MRI. J Magn Reson Imaging **24:**489–498.
33. **Lee VS, Hecht EM, Taoli B, Chen Q, Prince K, Oesingmann N.** 2007. Body and cardiovascular imaging at 3.0 T. Radiology **244:**692–705.
34. **Li T, Mirowitz SA.** 2003. T2-weighted echo planar MR imaging of the abdomen: optimization of imaging parameters. Clin Imaging **27:**124–128.
35. **Lin C, Luciani A, Itti E, Haioun C, Rahmouni A.** 2007. Whole-body MRI and PET/CT in haematological malignancies. Cancer Imaging **7 Spec No A:**S88–S93.
36. **Lin SP, Brown JJ.** 2007. MR contrast agents: physical and pharmacologic basics. J Magn Reson Imaging **25:**884–899.
37. **MacDonald KA, Wisner ER, Larson RF, Klose T, Kass PH, Kittleson MD.** 2005. Comparison of myocardial contrast enhancement in cardiac magnetic resonance imaging in healthy cats and cats with hypertrophic cardiomyopathy. Am J Vet Res **66:**1891–1894.
38. **Machann J, Schlemmer HP, Schick F.** 2008. Technical challenges and opportunities of whole-body magnetic resonance imaging at 3 T. Phys Med **24:**63–70.
39. **Machida T, Takahashi T, Itoh T, Hirayama M, Morita T, Horita S.** 2007. Reactive lymphoid hyperplasia of the liver: a case report and review of literature. World J Gastroenterol **13:**5403–5407.
40. **Martin DR, Friel HT, Danrad R, DeBecker J, Hussain SM.** 2005. Approach to abdominal imaging at 1.5 Tesla and optimization at 3 Tesla. Magn Reson Imaging Clin N Am **13:**241–254.
41. **Meyer JS.** 2008. Musculoskeletal imaging at 3 T: imaging and optimization. Pediatr Radiol **38:**S243–S245.
42. **Modiano JF, Breen M, Valli VE, Wojcieszyn JW, Cutter GR.** 2007. Predictive value of p16 or Rb inactivation in a model of naturally occurring canine nonHodgkin's lymphoma. Leukemia **21:**184–187.
43. **Mortele KJ, Rocha TC, Streeter JL, Taylor AJ.** 2006. Multimodal imaging of pancreatic and biliary congenital anomalies. Radiographics **26:**715–731.
44. **Newell SM, Graham JP, Roberts GD, Ginn PE, Chewning CL, Harrison JM, Andrzejewski C.** 2000. Quantitative magnetic resonance imaging of the normal feline cranial abdomen. Vet Radiol Ultrasound **41:**27–34.
45. **Nicoll RG, O'Brien RT, Jackson MW.** 1998. Qualitative ultrasonography of the liver in obese cats. Vet Radiol Ultrasound **39:**47–50.
46. **Nikken JJ, Krestin GP.** 2007. MRI of the kidney—state of the art. Eur Radiol **17:**2780–2793.
47. **Okada T, Mibayashi H, Hasatani K, Hayashi Y, Tsuji S, Kaneko Y, Yoshimitsu M.** 2009. Pseudolymphoma of the liver associated with primary biliary cirrhosis: a case report and review of literature. World J Gastroenterol **15:**4587–4592.

48. **Padhani AR, Koh DM, Collins DJ.** 2011. Whole-body diffusion-weighted MR imaging in cancer: current status and research directions. Radiology **261:**700–718.
49. **Penninck DG, Nyland TG, Fischer PE, Ker LY.** 1989. Ultrasonography of the normal canine gastrointestinal tract. Vet Radiol **30:**272–276.
50. **Robinson PJ.** 2009. The effects of cancer chemotherapy on liver imaging. Eur Radiol **19:**1752–1762.
51. **Samii VF, Biller DS, Koblik PD.** 1999. Magnetic resonance imaging of the normal feline abdomen: an anatomic reference. Vet Radiol Ultrasound **40:**486–490.
52. **Selvanayagam JB, Hawkins PN, Paul B, Myerson SG, Neubauer S.** 2007. Evaluation and management of the cardiac amyloidosis. J Am Coll Cardiol **50:**2101–2110.
53. **Schmidt GP, Kramer H, Reiser MF, Glaser C.** 2007. Whole-body magnetic resonance imaging and positron emission tomography–computed tomography in oncology. Top Magn Reson Imaging **18:1**93–202.
54. **Siegelman ES, Outwater EK.** 1999. Tissue characterization in the female pelvis by means of MR imaging. Radiology **212:**5–18.
55. **Taouli B, Ehman RL, Reeder SB.** 2009. Advanced MRI methods for assessment of chronic liver disease. Am J Roentgenol **193:**14–27.
56. **Tchelepi H, Ralls PW, Radin R, Grant E.** 2002. Sonography of diffuse liver disease. J Ultrasound Med **21:**1023–1032.
57. **Tefferi A, Vardiman JW.** 2009. Myelodysplatic syndromes. N Engl J Med **361:**1872–1885.
58. **Tsushima Y, Takano A, Taketomi-Takahashi A, Endo K.** 2007. Body diffusion-weighted MR imaging using high b-value for malignant tumor screening: usefulness and necessity of referring to T2-weighted images and creating fusion images. Acad Radiol **14:**643–650.
59. **Vail DM, Young KM.** 2007. Canine lymphoma and lymphoid leukemia, p 699–733. In: Withrow SJ, Vail DM. Withrow and MacEwen's small animal clinical oncology, 4th ed. Philadelphia (PA): Saunders.
60. **Walter PA, Feeney DA, Johnston GR, O'Leary T.** 1987. Ultrasonographic evaluation of spontaneous renal disease in dogs: 32 cases (1981–1986). J Am Vet Med Assoc **191:**999–1007.
61. **Walter PA, Johnston GR, Feeney DA, O'Brien T.** 1988. Applications of ultrasonography in the diagnosis of parenchymal kidney disease in cats: 24 cases (1981–1986). J Am Vet Med Assoc **192:**92–98.
62. **Weiss DJ.** 2005. Recognition and classification of dysmyelopoiesis in the dog: a review. J Vet Intern Med **19:**147–154.
63. **Yeager AE, Mohammed H.** 1992. Accuracy of ultrasonography in the detection of severe hepatic lipidosis in cats. Am J Vet Res **53:**597–599.
64. **Zhu J, Xu JR, Gong HX, Zhou Y.** 2008. Updating magnetic resonance imaging of small bowel: imaging protocols and clinical indications. World J Gastroenterol **14:**3403–3409.